SUPPORTING INFORMATION for

Mapping the molecular surface of the analgesic Na$_V$1.7-selective peptide Pn3a reveals residues essential for membrane and channel interactions

Alexander Mueller[a], Zoltan Dekan[a], Quentin Kaas[a], Akello J. Agwa[a,$], Hana Starobova[a], Paul F. Alewood[a], Christina I. Schroeder[a], Mehdi Mobli[b], Jennifer R. Deuis[a,*,1] and Irina Vetter[a,c,*,2]

[a]Institute for Molecular Bioscience, The University of Queensland, St. Lucia, QLD 4072, Australia

[b]Centre for Advanced Imaging, The University of Queensland, St. Lucia, QLD 4072, Australia

[c]School of Pharmacy, The University of Queensland, Woolloongabba, QLD 4102, Australia

[*] Co-corresponding authors

[1]Address: Institute for Molecular Bioscience, The University of Queensland, 306 Carmody Rd, St Lucia, Queensland 4072, Australia. Tel.: +617 3346 2721; E-mail: j.deuis@uq.edu.au

[2]Address: Institute for Molecular Bioscience, The University of Queensland, 306 Carmody Rd, St Lucia, Queensland 4072, Australia. Tel.: +617 3346 2660; fax: +61 733 462 101; E-mail: i.vetter@uq.edu.au

[$] Current address: University of Bath, Department of Biology and Biochemistry, BA27AY, Bath, UK.

The PDF file includes:

SUPPLEMENTARY MATERIALS AND METHODS

Surface Plasmon Resonance

Small unilamellar vesicles (SUVs) were prepared using POPC (1-palmitoyl-2-oleoyl-*sn*-glycero-3-phosphocholine) or a mix of POPC/POPS (1-palmitoyl-2-oleoyl-*sn*-glycero-3-phospho-$_L$-serine; 4:1 molar ratio) by combining with spectroscopic grade chloroform, drying under a stream of N_2, and further *in vacuo* for at least 3 h. Lipids were then re-suspended in HEPES buffered saline (HBS) (10 mM HEPES, 150 mM NaCl; pH 7.4), submitted to 8 freeze-thaw cycles, then extruded through a 50 nm polycarbonate filter to form SUVs [1-3]. Rationale for the choice of lipid bilayers has been discussed in detail previously [4, 5]. Briefly, POPC was used because lipids containing zwitterionic phosphatidylcholine headgroups are the most abundant on the outer leaflet of mammalian cells [6], and a mix of POPC/POPS (4:1) was used because phosphatidylserine headgroups represent anionic moieties on the cell surface [1, 4, 7, 8].

Peptide–lipid bilayer interactions were examined using surface plasmon resonance (SPR) on a BIAcore 3000 (GE Healthcare) using previously described protocols [1-3, 5]. HBS was used as running buffer and to prepare lipids and peptides. POPC and POPC/POPS (4:1) SUVs were deposited onto the surface of an L1 sensor chip at 2 μL/min for 43 min [8]. Peptides were then injected onto the lipid surface at 2 μL/min in concentrations ranging from 0–64 μM and association was monitored for 170 s followed by a dissociation phase. Response units (RU) were normalized to the molar quantity of peptides and lipids (peptide/lipid (mol/mol)) assuming 1RU = 1 pg/mm^2 of lipid and peptide, as previously described [2]. Concentration–response curves were obtained by fitting the data using a one-site specific binding curve using GraphPad Prism v7.00. Binding kinetic curves were fitted using association then dissociation curves on GraphPad Prism v7.00 [1].

SUPPLEMENTARY RESULTS AND DISCUSSION

Membrane Binding Properties of Pn3a and Analogues

Besides direct channel interactions, membrane affinity also appears to play an important role in the activity of some Na_V blockers [4] and has been well studied for e.g. ProTx-II, HwTx-IV and GpTx-1 [1, 8, 9]. However, nothing is known about the membrane binding properties of Pn3a. We therefore assessed the lipid bilayer affinity for Pn3a as well as the analogues D8N, D8K, K24R and K24D using surface plasmon resonance (SPR) to investigate a potential correlation between $Na_V1.7$ potency, surface charge changes and affinity for model lipid membranes.

The amount of peptide bound to lipid (P/L max (mol/mol)) was consistently doubled in anionic model lipid bilayers compared to zwitterionic POPC lipid bilayers for each peptide (**Fig. S4**, **Table S2**). A preferential affinity for anionic lipid bilayers is typical for spider ICK peptides and suggests that electrostatic interactions drive the interactions between these peptides with lipid bilayers [1, 5, 8, 9]. Compared to Pn3a in POPC/POPS (4:1) model lipid bilayers, Pn3a[D8K] showed a combination of the most amount of peptide bound to lipid and strongest affinity (slowest dissociation), followed by Pn3a[D8N] (**Fig. S4**, **Table S2**). This demonstrates that removal of the anionic charge from position 8 improves attraction to the lipid bilayers and that a lysine residue is preferential to a polar uncharged asparagine, confirming that electrostatic interactions are most likely important for interactions with the lipid bilayer. Pn3a[K24D] and Pn3a[K24R] both showed a reduction in the amount of peptide bound to lipid compared to Pn3a, suggesting that in the absence of Na_V channels, K24 may be on the face of the peptide that interacts with the lipid bilayers, and that a lysine residue in position 24 is preferred to an arginine residue for attraction to lipid bilayers (**Fig. S4**, **Table S2**). However, while K24D significantly lost and K24R gained potency at $Na_V1.7$ (**Fig. 2B**, **Table 2**), neither peptides differ in their membrane binding properties, suggesting that the difference in activity at $Na_V1.7$ is driven by direct channel interactions of the mutated residue at position 24 rather than by membrane binding. Generally, Pn3a and all tested analogues show moderate affinity for model lipid bilayers compared to previously studied ICK peptides *i.e.* Pn3a had stronger affinity compared to peptides like HwTx-IV, SGTx-I and GpTx-I, similar affinity to ProTx-I, but less affinity for model lipid bilayers than ProTx-II or gHwTx-IV [1, 5, 8].

SUPPLEMENTARY FIGURES

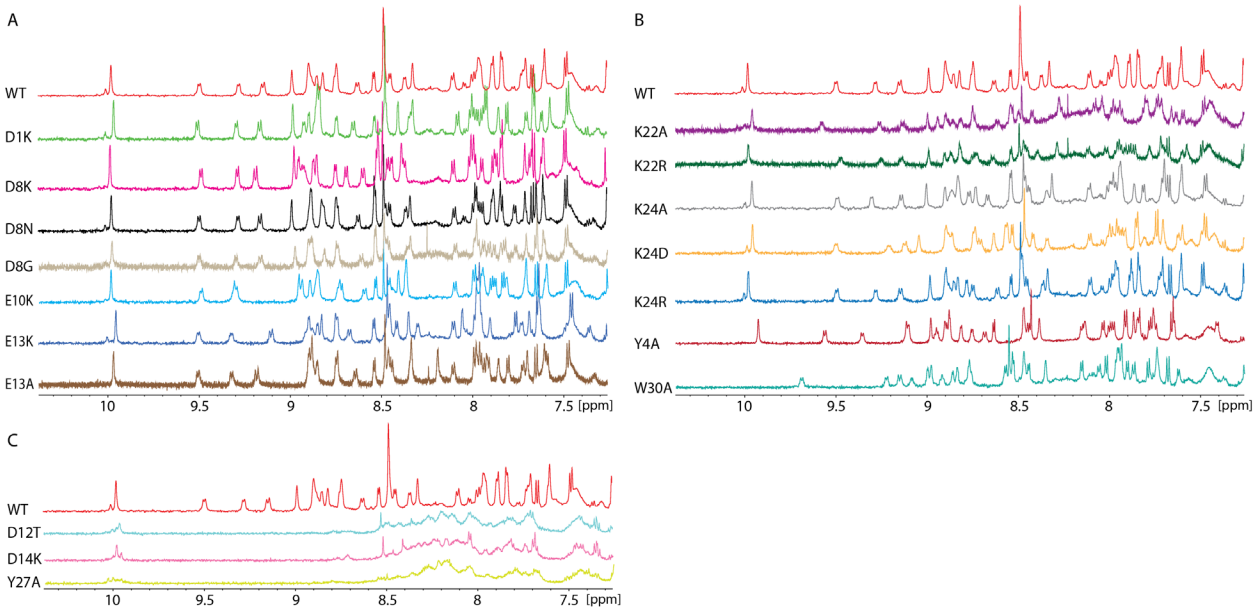

Figure S1. 1D NMR spectra of Pn3a analogues compared to Pn3a (WT). **(A)** Analogues with exchanges in acidic residues show similar resonance positions in the NH region, indicating a similar overall fold compared to native Pn3a. **(B)** Analogues with exchanges in basic and hydrophobic residues also adopt a Pn3a-like fold. The W30A mutation results in an expected stronger shift of resonance peaks in the NH region. **(C)** Analogues D12T, D14K and Y27A appear misfolded.

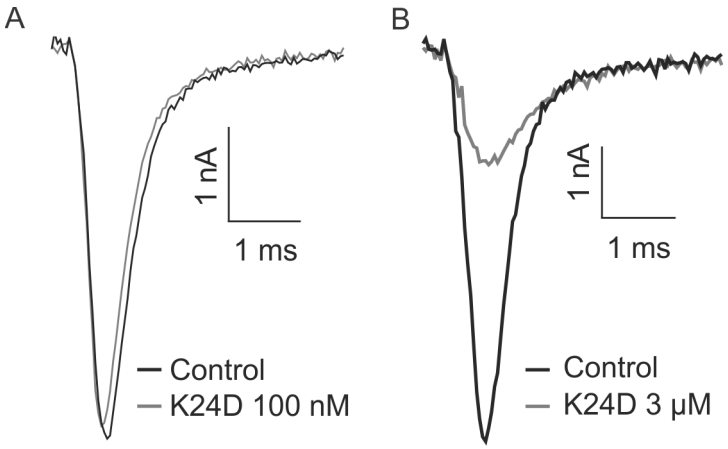

Figure S2. K24D does not inhibit inactivation of $Na_V1.7$ or $Na_V1.1$ channels in whole-cell patch-clamp experiments. **(A)** Current over time traces elicited by a 20 ms pulse from -90 mV to -20 mV before (black) and after (grey) addition of Pn3a[K24D] (100 nM) at $hNa_V1.7$ channels. **(B)** Current over time traces elicited by a 20 ms pulse from -90 mV to -20 mV before (black) and after (grey) addition of Pn3a[K24D] (3 µM) at $hNa_V1.1$ channels.

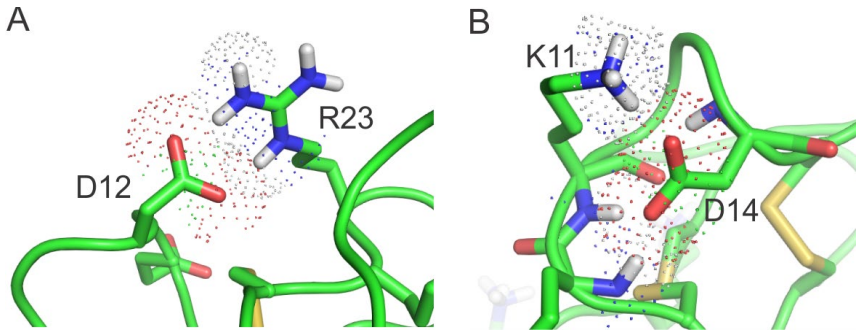

Figure S3. Intramolecular interactions of Pn3a (**A**) NMR structure of Pn3a (PDB 5T4R, green) indicates close interaction and a possible salt bridge between D12 and R23. (**B**) NMR structure of Pn3a indicates close interactions of D14 with backbone amides and K11. Residues of interest are labelled and shown in stick-representation. Visualization of data was generated with PyMol.

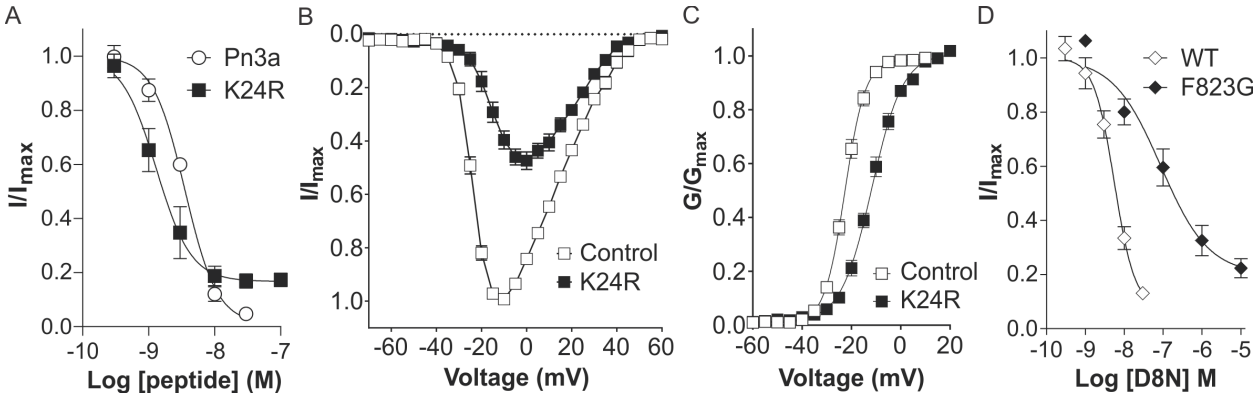

Figure S4. Pharmacological characterization of Pn3a analogues by whole-cell patch-clamp experiments. **(A)** Concentration response curve of wild-type Pn3a and Pn3a[K24R] at hNa$_V$1.7. **(B)** Current-voltage (IV) relationship before and after addition of Pn3a[K24R] (100 nM) at hNa$_V$1.7. **(C)** Conductance-voltage (GV) relationship before and after addition of Pn3a[K24R] (100 nM) at hNa$_V$1.7. Pn3a[K24R] shifted the voltage-dependence of activation by +11.0 mV (from –22.62 mV to –11.67 mV). **(D)** Pn3a[D8N] is 16-fold more potent at wild-type mNa$_V$1.7 (IC_{50} 5.6 nM) compared to mNa$_V$1.7[F823G] mutant channels (IC_{50} 87.4 nM). Data are presented as mean ± SEM, with n = 5–9 cells per data point.

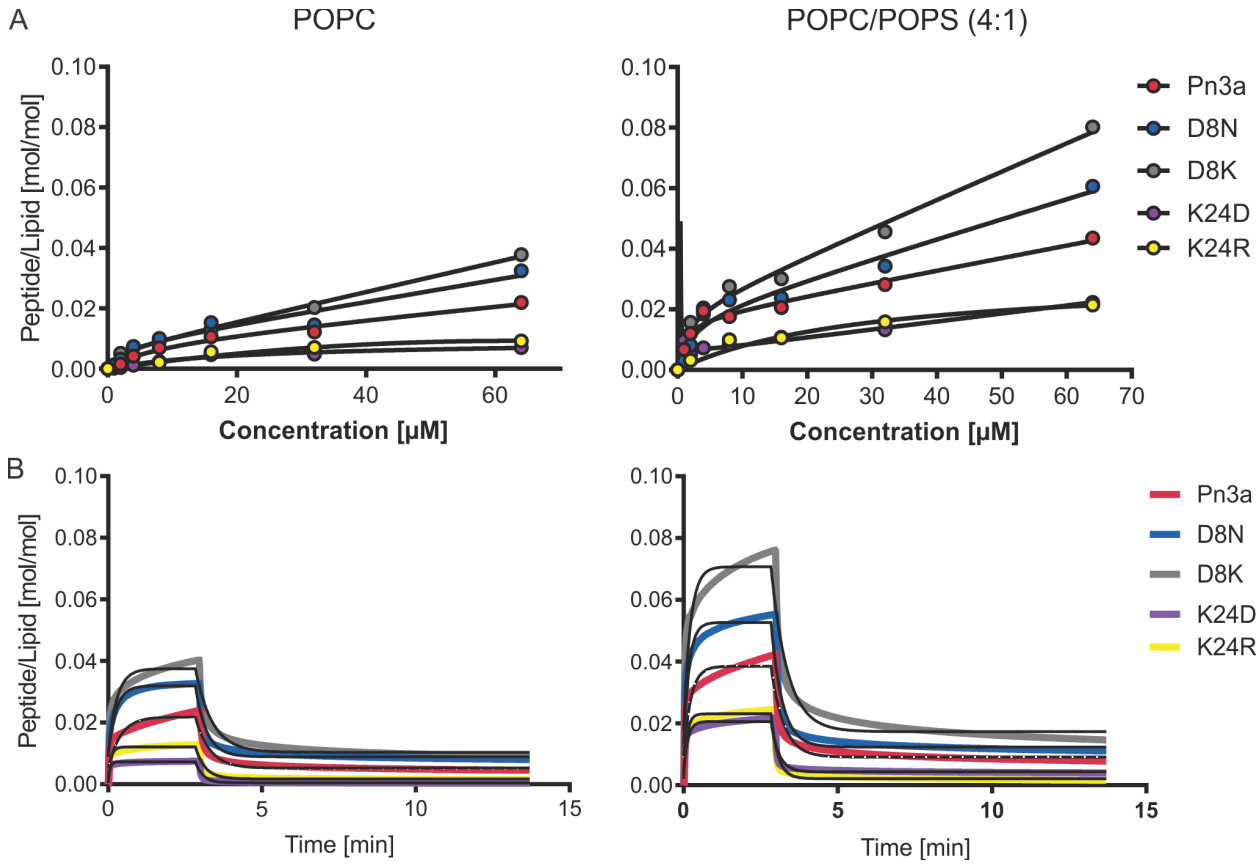

Figure S5. Peptide interactions with model lipid bilayers assessed by surface plasmon resonance (SPR). **(A)** Concentration–response curves of the peptides to POPC and POPC/POPS lipid bilayers, obtained by plotting the amount of peptide bound to lipid at each concentration after completion of peptide injection onto lipid (t = 170 s). **(B)** Sensorgrams showing association and dissociation of peptides (at 64 μM) over time. Lines of best-fit (R^2 >0.95) are shown in black and were determined using an association and dissociation fit, and dissociation is monitored starting at the end of peptide injection (t = 170 s). All data were corrected for contribution from buffer, normalized to molar quantities of peptides and lipids used and analyzed using GraphPad Prism v7.00.

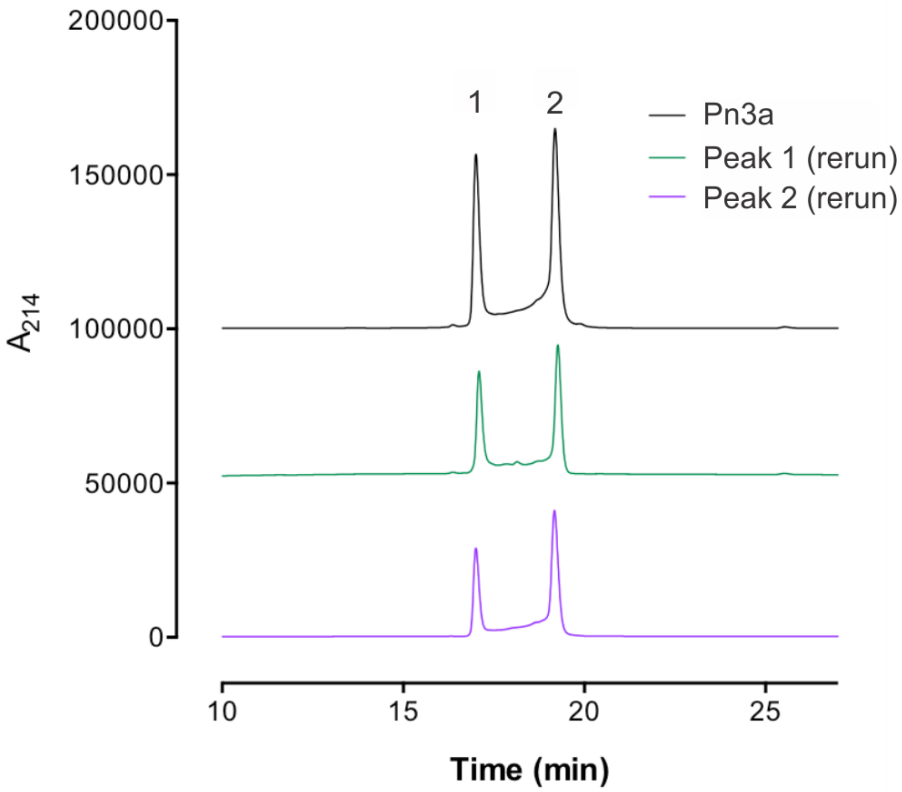

Figure S6. Analytical HPLC chromatogram of Pn3a. The chromatogram shows the typical elution profile of correctly folded Pn3a with two clean, well-separated symmetrical peaks. Collection and reanalysis of each individual peak via analytical HPLC results in reappearance of the same two peaks. All synthesized, purified Pn3a analogues produced the two clean, symmetrical peaks, with the exception of the misfolded peptides D12T, D14K and Y27A, which only showed single peaks in all the isolated fractions of the predominant isomers. Absorbance was measured at 214nm. Analytical HPLC was performed as detailed in [10].

Table S1. Potency of Pn3a analogues at Nav1.1-1.8 assessed using fluorescence-based assays[a]

	$Na_V1.1$	Na_V 1.2	Na_V 1.3	Na_V 1.4	Na_V 1.5	Na_V 1.6	Na_V 1.7	Na_V 1.8
Pn3a	5.74 ± 0.21	6.30 ± 0.09	4.86 ± 0.09	5.48 ± 0.08	< 4.52	< 4.52	7.03 ± 0.04	4.58 ± 0.03
Pn3a[D1K]	6.11 ± 0.17	6.58 ± 0.06	5.38 ± 0.22	5.57 ± 0.18	< 4.52	< 4.52	7.36 ± 0.06	4.72 ± 0.20
Pn3a[D8N]	6.46 ± 0.19	6.83 ± 0.13	5.54 ± 0.18	5.88 ± 0.26	< 4.52	< 4.52	7.82 ± 0.17	< 4.52
Pn3a[D8K]	6.62 ± 0.19	7.40 ± 0.10	5.69 ± 0.28	6.08 ± 0.23	< 4.52	< 4.52	7.85 ± 0.11	4.62 ± 0.10
Pn3a[E10K]	6.42 ± 0.17	6.76 ± 0.13	5.29 ± 0.21	5.67 ± 0.10	4.79 ± 0.11	6.11 ± 0.05	7.33 ± 0.15	< 4.52
Pn3a[E13K]	6.08 ± 0.17	6.43 ± 0.06	5.19 ± 0.25	5.58 ± 0.07	< 4.52	5.88 ± 0.17	7.21 ± 0.21	< 4.52
Pn3a[K24R]	6.06 ± 0.24	6.38 ± 0.06	5.09 ± 0.21	5.49 ± 0.17	< 4.52	< 4.52	7.46 ± 0.22	< 4.52

[a]Data is presented as the mean pIC_{50} ± SEM, averaged from 3–6 independent replicates (with three identically treated wells each) assessed by fluorescence-based assays.

Table S2. SPR values[a]

	POPC		POPC/POPS (4:1)	
Peptide	**P/L max**[b] **(mol/mol)**	**K_D**[c] **(μM)**	**P/L max**[b] **(mol/mol)**	**K_D**[c] **(μM)**
Pn3a	0.02	0.43 ± 0.16	0.04	0.08 ± 0.01
Pn3a[D8N]	0.03	0.13 ± 0.01	0.06	0.06 ± 0.005
Pn3a[D8K]	0.04	0.07 ± 0.01	0.08	0.04 ± 0.003
Pn3a[K24D]	0.01	0.02 ± 0.001	0.02	0.07 ± 0.01
Pn3a[K24R]	0.01	0.03 ± 0.002	0.02	0.06 ± 0.01

[a]Data is presented as mean ± SEM

[b]P/L max is the ratio of the amount of peptide bound to lipid (mol/mol) at the end of the association phase (t = 170 s) for 64 μM of peptide

[c]$K_D = K_{off}/K_{on}$ and was calculated for 64 μM peptide by following association (K_{on} ($min^{-1} \bullet \mu M^{-1}$)) then dissociation K_{off} (min^{-1}) on GraphPad Prism v7.00

Table S3: Calculated and measured molecular weight of Pn3a analogues[a]

Pn3a analogue	Calculated mass [Da]	Observed mass [Da]
WT	4271.9	4271.7
D1K	4285.0	4285.2
Y4A	4179.8	4179.6
D8K	4285.0	4284.6
D8N	4271.0	4270.8
D8G	4213.9	4213.5
E10K	4271.0	4271.4
D12T[b]	4257.9	4258.2
E13K	4271.0	4271.1
E13A	4213.9	4213.2
D14K[b]	4285.0	4284.9
K22A	4214.8	4214.7
K22R	4299.9	4299.9
K24A	4214.8	4215.0
K24D	4258.8	4259.1
K24R	4299.9	4299.3
Y27A[b]	4179.8	4179.9
W30A	4156.8	4156.5

[a] Peptides were analyzed via electrospray ionization mass spectrometry as previously described [10]. Data is presented as average mass. The observed mass of all peptides corresponded with their calculated mass.
[b]Non-native fold assessed by 1D NMR; all other analogues showed a similar fold to WT peptide.

SUPPORTING INFORMATION REFERENCES

[1] Agwa, A. J., Lawrence, N., Deplazes, E., Cheneval, O., Chen, R. M., Craik, D. J., Schroeder, C. I., and Henriques, S. T. (2017) Spider peptide toxin HwTx-IV engineered to bind to lipid membranes has an increased inhibitory potency at human voltage-gated sodium channel hNa$_V$1.7, *Biochimica et biophysica acta. Biomembranes 1859*, 835-844. DOI: 10.1016/j.bbamem.2017.01.020

[2] Henriques, S. T., Huang, Y. H., Rosengren, K. J., Franquelim, H. G., Carvalho, F. A., Johnson, A., Sonza, S., Tachedjian, G., Castanho, M. A., Daly, N. L., and Craik, D. J. (2011) Decoding the membrane activity of the cyclotide kalata B1: the importance of phosphatidylethanolamine phospholipids and lipid organization on hemolytic and anti-HIV activities, *J Biol Chem 286*, 24231-24241. DOI: 10.1074/jbc.M111.253393

[3] Henriques, S. T., Pattenden, L. K., Aguilar, M. I., and Castanho, M. A. (2008) PrP(106-126) does not interact with membranes under physiological conditions, *Biophysical journal 95*, 1877-1889. DOI: 10.1529/biophysj.108.131458

[4] Agwa, A. J., Henriques, S. T., and Schroeder, C. I. (2017) Gating modifier toxin interactions with ion channels and lipid bilayers: Is the trimolecular complex real?, *Neuropharmacology 127*, 32-45. DOI: 10.1016/j.neuropharm.2017.04.004

[5] Agwa, A. J., Peigneur, S., Chow, C. Y., Lawrence, N., Craik, D. J., Tytgat, J., King, G. F., Henriques, S. T., and Schroeder, C. I. (2018) Gating modifier toxins isolated from spider venom: Modulation of voltage-gated sodium channels and the role of lipid membranes, *J Biol Chem 293*, 9041-9052. DOI: 10.1074/jbc.RA118.002553

[6] van Meer, G., and de Kroon, A. I. (2011) Lipid map of the mammalian cell, *J Cell Sci 124*, 5-8. DOI: 10.1242/jcs.071233

[7] Deplazes, E., Henriques, S. T., Smith, J. J., King, G. F., Craik, D. J., Mark, A. E., and Schroeder, C. I. (2016) Membrane-binding properties of gating modifier and pore-blocking toxins: Membrane interaction is not a prerequisite for modification of channel gating, *Biochimica et biophysica acta. Biomembranes 1858*, 872-882. DOI: 10.1016/j.bbamem.2016.02.002

[8] Henriques, S. T., Deplazes, E., Lawrence, N., Cheneval, O., Chaousis, S., Inserra, M., Thongyoo, P., King, G. F., Mark, A. E., Vetter, I., Craik, D. J., and Schroeder, C. I. (2016) Interaction of tarantula venom peptide ProTx-II with lipid membranes is a prerequisite for its inhibition of human voltage-gated sodium channel Na$_V$1.7, *J Biol Chem 291*, 17049-17065. DOI: 10.1074/jbc.M116.729095

[9] Lawrence, N., Wu, B., Ligutti, J., Cheneval, O., Agwa, A. J., Benfield, A. H., Biswas, K., Craik, D. J., Miranda, L. P., Henriques, S. T., and Schroeder, C. I. (2019) Peptide-membrane interactions affect the inhibitory potency and selectivity of spider toxins ProTx-II and GpTx-1, *ACS Chem Biol 14*, 118-130. DOI: 10.1021/acschembio.8b00989

[10] Mueller, A., Starobova, H., Morgan, M., Dekan, Z., Cheneval, O., Schroeder, C. I., Alewood, P. F., Deuis, J. R., and Vetter, I. (2019) Antiallodynic effects of the selective Na$_V$1.7 inhibitor Pn3a in a mouse model of acute postsurgical pain: evidence for analgesic synergy with opioids and baclofen, *Pain 160*, 1766-1780. DOI: 10.1097/j.pain.0000000000001567